https://doi.org/10.5194/egusphere-2025-6340
Preprint. Discussion started: 30 December 2025

Atlantic Water flow through Fram Strait to the Arctic Ocean measured by repeated glider transects

Vår Dundas[1, a] and Ilker Fer[1]

[1]Geophysical Institute, University of Bergen, and Bjerknes Centre for Climate Research, Bergen, Norway
[a]Now at Nansen Environmental and Remote Sensing Center, Bergen, Norway

Correspondence: Ilker Fer (ilker.fer@uib.no)

Abstract. We present estimates of northward transport of Atlantic Water (AW) across a zonal transect at $77°15'$N using repeated ocean glider observations. Over three missions during autumn and winter of 2020–2022, 22 high-resolution sections were collected, enabling detailed characterization of circulation branches and volume transport. On average, the West Spitsbergen Current (WSC) and the Front Current each transport approximately $2.5\,\mathrm{Sv}$ of AW ($\Theta > 2°\mathrm{C}$, $S_A > 35.06\,\mathrm{g\,kg^{-1}}$) northward, yielding a combined flux of about $5\,\mathrm{Sv}$ toward the Arctic. Variability in transport and current structure is substantial and appears linked to atmospheric forcing. Case studies reveal that anomalous northward wind stress coincides with peak AW transport, roughly twice the seasonal mean, consistent with Ekman dynamics and elevated sea surface height along the coast. Conversely, strong southward wind stress weakens the WSC and nearly eliminates the Front Current. Recirculating Atlantic Water (RAW, $\Theta > 0°\mathrm{C}$, $S_A > 35.06\,\mathrm{g\,kg^{-1}}$) west of the Front Current is estimated to be about $1\,\mathrm{Sv}$, but this does not capture the expected stronger recirculation transport further west, beyond the glider's target transect. These results highlight the capability of gliders to resolve variability in boundary currents that mooring arrays cannot capture. Extended seasonal coverage, including summer, is needed to assess transport variability under peak wind forcing.

1 Introduction

Poleward flow of Atlantic Water (AW) from the Nordic Seas is the main contributor of oceanic heat and salt into the Arctic Ocean (Aagaard et al., 1987; Rudels, 2015), with far reaching effects on sea ice cover, ocean stratification and ecological environments (Ingvaldsen et al., 2021; Polyakov et al., 2025). Fram Strait, located between Greenland and Svalbard, is the deepest connection between the Arctic Ocean and the Nordic Seas, and the main pathway for AW into the Arctic.

The circulation patterns of AW in Fram Strait are complex (Fig. 1). To monitor the ocean currents, and temperature and salinity structure in this passage, an array of oceanographic moorings has been maintained at $78°50'$–$79°$ N since 1997 as a joint effort between the Alfred Wegener Institute and the Norwegian Polar Institute (Schauer et al., 2004; Beszczynska-Möller et al., 2012). The measurements from this array have been used to quantify the volume and heat fluxes, and their variability at this section. These moorings have provided observations with high temporal resolution over long time periods, and given insight into long-term changes as well as seasonal and short-term variability in circulation and hydrography in Fram Strait (Beszczynska-Möller et al., 2012; von Appen et al., 2016). The lateral and vertical resolution of instrumentation in the mooring

https://doi.org/10.5194/egusphere-2025-6340
Preprint. Discussion started: 30 December 2025

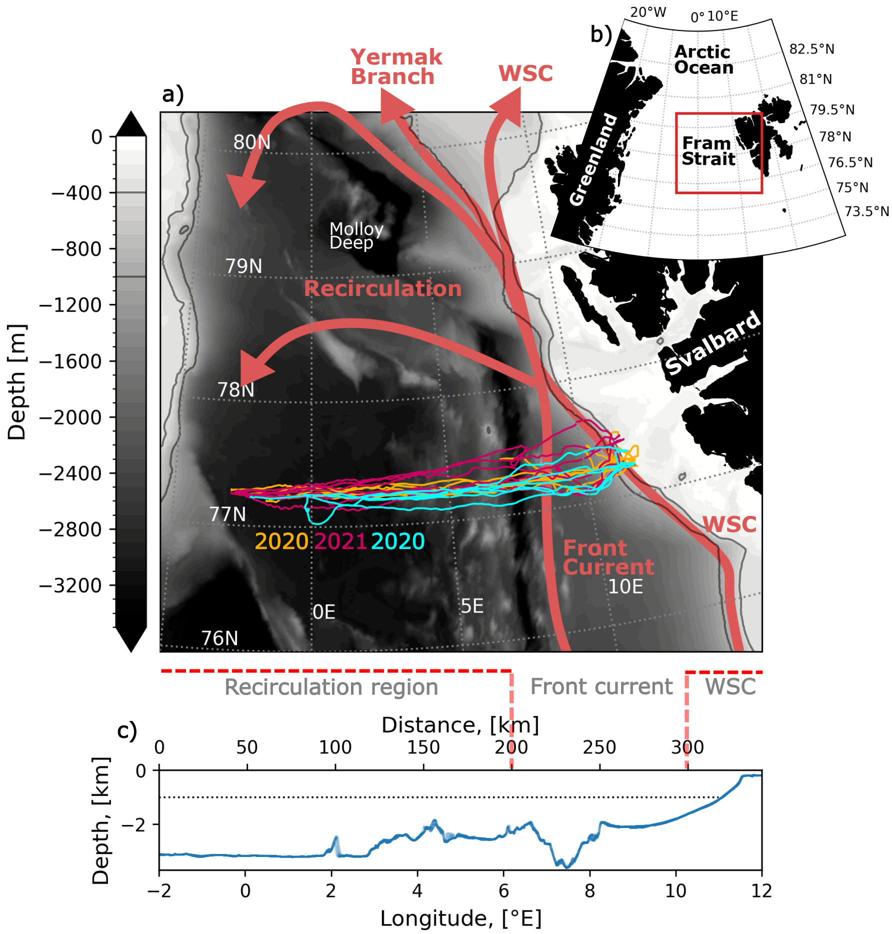

Figure 1. a) Bathymetry in Fram Strait (Jakobsson et al., 2020) including sections from glider mission 1 (2020, yellow), mission 2 (2021, pink), and mission 3 (2022, cyan). Circulation pattern of the warm Atlantic current including the West Spitsbergen Current (WSC), the Front Current, the Yermak Branch and recirculation branches are indicated based on our observations and observations from the literature. Gray isobaths are −400 m and −1000 m. b) The inset in the upper right corner shows the location of our study region and panel a) is bounded by the red box. c) The bathymetry along the target section. The dotted black line indicates the glider's maximum depth of 1000 m. Selected boundaries at 200 km and 300 km distance along the transect (dashed red lines) delineate the different current regions.

https://doi.org/10.5194/egusphere-2025-6340
Preprint. Discussion started: 30 December 2025

array is, however, relatively coarse and does not capture the detailed structure of currents and hydrography. Here, we analyze observations from repeated ocean glider sections taken during three consecutive years (Fer et al., 2025) with the aim to resolve the lateral and vertical structure of the AW flow and its variability in Fram Strait. These observations have a horizontal length scale of order 1 km and vertical scales of 1 m, which complements the high temporal resolution provided by the mooring array.

AW is brought into Fram Strait by the Norwegian Atlantic Current system comprised of the Norwegian Atlantic Slope Current flowing along the shelf break of Norway and the Barents Sea opening, and the Norwegian Atlantic Front Current following the Mohn and Knipovich ridges (Orvik and Niiler, 2002). Both branches are guided by topography, but the front current is a surface-intensified baroclinic jet, while the slope current is more barotropic. Along the southern West Spitsbergen Shelf edge, the slope current is referred to as the West Spitsbergen Current (WSC). Along the west coast of Svalbard, parts of the AW carried by the WSC can diverge from its core, intruding eastward onto the West Spitsbergen Shelf and further toward the adjacent fjords (Frank et al., 2025), effecting the regional hydrography, marine biosphere, sea ice variability as well as melting and calving rates of marine-terminating glaciers. As the offshore topographic contours converge near 78°N, the Front Current branch merges into the WSC (Orvik and Niiler, 2002; Walczowski et al., 2005). Approximately half of the AW in Fram Strait enters the Arctic Ocean whereas the remaining AW recirculates and joins the southward flowing East Greenland Current (Quadfasel et al., 1987; Manley, 1995; Dale et al., 2024). As a consequence of the recirculation, warm temperature anomalies in the WSC partly control Atlantic Water temperatures on the Northeast Greenland continental shelf, which in turn control the melt rate of major glaciers in the region (McPherson et al., 2023).

Based on the mooring observations, the average structure of the currents carrying AW at 79° N can be described by three components: i) The WSC core (or the Svalbard branch), which is an extension of the slope current and flows on the upper shelf slope, ii) an outer offshore branch which is an extension of the front current and extends to the foot of the shelf slope, and iii) several recirculating branches mid-strait (Fig. 1a, Beszczynska-Möller et al., 2012). The outer branch is referred to as the Yermak branch north of 79°N. Recirculation of AW captured by moorings along the prime meridian is relatively continuous at $78°50'$N, but is characterized by passing eddies at $80°10'$N (Hofmann et al., 2021). Eddy-resolving numerical models show that the bulk of the recirculation occurs along two pathways between 78°N and 81°N (Hattermann et al., 2016; Wekerle et al., 2017): one along the Spitsbergen Fracture Zone and south of the Molloy Hole and the other is located along the Molloy Fracture Zone and north of the Molloy Hole (Fig. 1a).

At the Fram Strait mooring array, the average (1997–2010) northward volume transport of water warmer than 2°C is 3.0 ± 0.2 Sv (Sverdrup, 1 Sv $\equiv 10^6$ m^{3}s^{-1}), showing a strong seasonal signal with summer averages approximately doubling in late autumn and winter (Beszczynska-Möller et al., 2012). Out of these 3 Sv, 1.3 ± 0.1 Sv is carried in the WSC core (Beszczynska-Möller et al., 2012). Further north, year-round observations from moorings on the southern slope of the Yermak Plateau show an average AW transport of 1.1 ± 0.2 Sv with a maximum in autumn (1.4 ± 0.2 Sv), and a minimum in summer (0.8 ± 0.1 Sv, Fer et al., 2023).

Moorings provide highly valuable time series of oceanic conditions, but their limited lateral and vertical resolution introduces substantial uncertainty in AW transport estimates. For instance, moorings may fail to capture the current core, leading to underestimation of AW fluxes, while coarse estimates of current width can result in both over- and underestimations. It is also

https://doi.org/10.5194/egusphere-2025-6340
Preprint. Discussion started: 30 December 2025

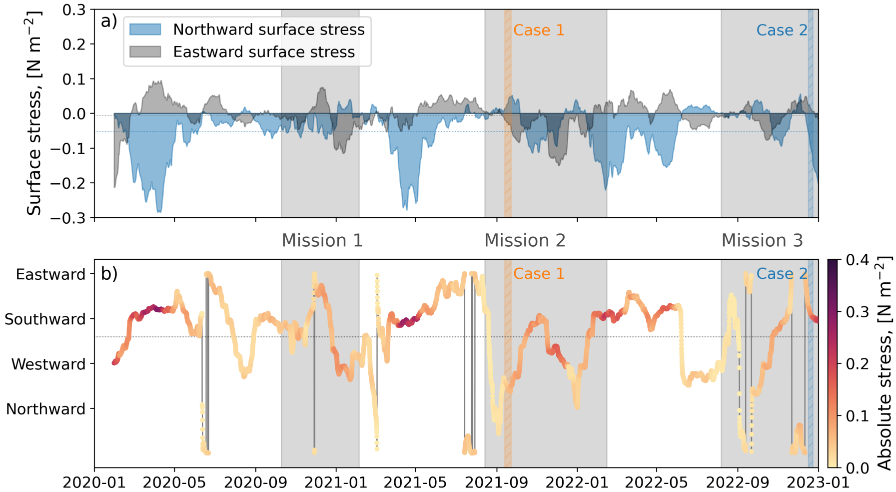

Figure 2. 30-day rolling averages of surface stress (Hersbach et al., 2023) averaged over 2°W – 12°E at 77°N. a) Northward (blue) and eastward (grey) average surface stress, and b) its direction (grey line) and absolute magnitude (color). In both panels, the mission periods are indicated with grey background and the two case study periods are indicated by orange and blue hatched bars. The thin dotted horizontal lines in a) indicate the mean northward (blue) and eastward (grey) stress, and b) the mean stress direction (grey).

difficult to determine whether observed fluctuations in current strength and hydrographic properties reflect lateral shifts in the core's position or actual changes in its properties. Ship-based hydrographic and current sections help address these questions, but such data are scarce. Repeated observations with high lateral and vertical resolution are essential, yet traditionally lacking. Ocean gliders help fill this gap by providing data with the required spatial coverage and resolution.

Ocean gliders (gliders hereafter) have become widely-used platforms enabling ocean research and sustained observation at relatively fine horizontal scales (Rudnick, 2016). A glider is a buoyancy-driven, remotely-piloted autonomous vehicle, which profiles in a sawtooth trajectory as it travels between way points (Eriksen, 2001; Rudnick, 2016; Testor et al., 2019). A glider changes its buoyancy to profile vertically, typically to 1000 m depth and slanted at 20 to 30°. Wings generate hydrodynamic lift force with a horizontal component propelling the glider horizontally. A glider covers $\mathcal{O}(100)$ km transects (e.g. covering a boundary current) in about 4 days, providing profiles with horizontal separation of 1 to 4 km and vertical resolution of 1 to 5 m.

Here, we use fine-resolution spatial data from gliders that transected Fram Strait in autumn and winter between 2020 and 2022 to estimate northward AW volume transport and recirculation. We present average current and hydrography fields, and the AW volume transport associated to the WSC, the Front Current and the recirculation region throughout the glider missions in 2020-2022, and associate characteristic zonal AW transport structures to atmospheric forcing.

https://doi.org/10.5194/egusphere-2025-6340
Preprint. Discussion started: 30 December 2025

2 Data and methods

2.1 Glider data

We present data from three glider missions in Fram Strait, conducted between October 2020 and February 2023, using 1000-m rated Seagliders, operated by the Norwegian Facility for Ocean Gliders at the Geophysical Institute, University of Bergen. Seaglider is a widely-used type of ocean glider (Eriksen, 2001). The glider data are available from Fer et al. (2025), which include detailed description of data processing, calibration and quality control.

The target section was selected to capture the front and slope branches before they merge, enabling separate estimates of their volume transport and variability. It was located at $77°15'$N between 2°W to 12°E. In 3 missions, a total of 22 sections were collected. Of these, only five sections are incomplete, mainly due to recovery and deployment constraints. Mission details are summarized in Table 1.

During the first mission (7 October 2020 – 8 February 2021), the glider completed 625 dives and collected 1250 profiles before entering recovery mode. The second mission (3 August 2021 – 10 March 2022) included 805 dives (1610 profiles), with science operations ending on 20 February. The third mission (22 July 2022 – 8 February 2023) performed 960 dives (1920 profiles), but science data collection stopped after dive 715 (profile 1430) on 2 January to conserve battery for recovery. Each mission was separated by a five to six month gap, and coverage was primarily during autumn and winter.

The gliders operated between the surface and 1000 m depth, or 10 to 15 m above seafloor for shallower depths, sampling during both dives and climbs. The vertical velocity was typically $10\,\mathrm{cm\,s^{-1}}$. The gliders were equipped with a Kistler pressure sensor, a Sea-Bird Scientific CT Sail (unpumped) measuring conductivity and temperature, and an Aanderaa dissolved oxygen sensor. The sampling rate of the sensors was variable. Typically the CT sail sampled every 10 s in the upper 300 m, 15 s between 300 m and 600 m, and 20 s between 600 m and 1000 m. The optode sampled a factor of five slower, every 50 s, 75 s and 100 s, respectively. The vertical resolution of the temperature and conductivity profiles are $\sim$1 m in the upper 300 m and $\sim$1.5 m from 300 m to 600 m. The data set was processed using the Seaglider Basestation3 (v3.0.4) software, including a hydrodynamic flight model regression, correction for the thermal lag of the conductivity cell, and quality control. Temperature and salinity profiles, as well as the derived density, are quality controlled, first using automated routines, and then applying additional despiking and manual quality control, as detailed in the data files. Absolute Salinity S_A, Conservative Temperature Θ, and potential density anomaly σ_0 are obtained using TEOS-10 and the Gibbs Seawater toolbox for Python (McDougall and Barker, 2011).

In our data set, the mean ($\pm$ one standard deviation) horizontal spacing at the surface of subsequent downward (dive) and upward (climb) profiles was 3.5 ± 2.3 km and roughly 5.3 ± 2.0 h. The spacing of the profiles is primarily set by the profiling depth, which ranged from roughly 150 m to 1000 m (99% of all profiles were deeper than 150 m). The repeat cycle of the target section is 7 to 36 days. The main reason for this large range are the five incomplete sections.

After initial processing, the data were averaged onto the target section using bins of 2 km in width and 2 dbar in pressure (approximately 2 m depth). The section spans 342 km in longitude. We define the horizontal eastward distance along the target section starting from 2°W and refer to it as “distance” hereafter. For data west of 300 km, gridding is based on longitude

https://doi.org/10.5194/egusphere-2025-6340
Preprint. Discussion started: 30 December 2025

Table 1. Deployment details for the three missions. The “stop” date is the date of the last good profile. Additional information can be found in the metadata of the data files in Fer et al. (2025).

	Glider	Start	Stop	Profiles	Sections
Mission 1	sg562	7 Oct 2020	7 Feb 2021	1250	7
Mission 2	sg560	3 Aug 2021	20 Feb 2022	1610	7
Mission 3	sg560	22 Jul 2022	2 Jan 2023	1430	8

because there are no major bathymetric constraints in this region. East of 300 km ($\sim$ 1600 m isobath), however, currents are strongly influenced by the steep bathymetry near the continental shelf break. In this region, gridded averaging is referenced to bathymetry: each profile is assigned to its isobath and shifted to the nearest corresponding isobath on the target section. Profiles sampled more than 30 km away from the target section are discarded.

We construct horizontal distance versus depth sections of measured variables using an objective interpolation algorithm using the GliderTools package for Python (Gregor et al., 2019). We estimate horizontal (40 km) and vertical (40 m) length scales, the nuggets (temperature: 0.1075, salinity: 0.0012) and partial sills (temperature: 0.3105, salinity: 0.0025) using GliderTool’s semivariance function over a region that captures northward Atlantic Water variability (20 to 200 m depth and 230 to 340 km distance). These parameters are then applied for objective mapping of the gridded data fields to the target section. We thus have 22 mapped sections of the target transect.

2.2 Geostrophic currents

Geostrophic shear of the horizontal velocity component perpendicular to the target section is calculated from the thermal wind equation, using the horizontal slope of density surfaces from the final gridded and objectively interpolated glider data with the Gibbs Seawater (GSW) Oceanographic Toolbox (McDougall and Barker, 2011). The smoothing length scales applied to the hydrographic data are appropriate for geostrophic calculations.

To obtain absolute geostrophic currents, accurate reference currents representative of barotropic flow are required. Typically, glider-based depth-averaged currents (DAC) over the upper 1000 m, smoothed over the same horizontal scale as the hydrographic data, can be used. However, during the first half of the second mission, DAC estimates exhibit erroneous values: northward currents are anomalously strong across the full transect for several months (Fig. A1b), a pattern not confirmed by independent ocean monitoring and forecasting fields from the Copernicus Marine Service or by mooring data at 79° N (Rebecca McPherson, personal communication, 14 November 2024).

Outside this period, depth-averaged currents from the glider agree well with surface geostrophic currents from the gridded altimeter product (Global Ocean Gridded L4 Sea Surface Heights And Derived Variables Reprocessed 1993 Ongoing, 2024) calculated from the slope of the absolute dynamic height using a geostrophic balance (Fig. A1). Therefore, for consistency, we combine baroclinic currents estimated from glider hydrography data with the surface geostrophic currents from the altimeter product for all sections to obtain absolute geostrophic currents.

https://doi.org/10.5194/egusphere-2025-6340
Preprint. Discussion started: 30 December 2025

Mork and Skagseth (2010) used repeated hydrographic data in the Svinøy section (at 62°N off the coast of Norway) with absolute dynamic sea surface topography data to quantify the mean flow and the variability in the slope and front branches of the Norwegian Atlantic Current. For the slope branch, the estimated currents agreed well with the current measurements within the error range, but they were approximately 15% lower and the lateral structure was smoother, as a result of the relatively coarse resolution and the gridding of the altimeter data. We expect comparable underestimates for the volume transports in our data. Excluding the first half of Mission 2 (sections 7 to 10) with erroneous DAC estimates, the difference between the volume transports estimated using DAC from the glider and the surface current from the altimetry is generally less than one standard deviation of the two estimates (not shown), lending credibility for using the satellite derived values for the full data set.

2.3 Atmospheric forcing

To investigate the relationship between atmospheric forcing and the oceanic variability observed in the glider data, we use hourly output of wind stress and sea ice concentration from ERA5 reanalysis (Hersbach et al., 2023). Wind stress curl is estimated from the wind stress vector and the uniform $0.25° \times 0.25°$ horizontal resolution, using $\nabla \times \tau = \Delta\tau_y/\Delta x - \Delta\tau_x/\Delta y$. When presenting zonal sections of wind stress and wind stress curl we average meridionally between $76°30'$N and $78°$N and temporally over the time it took the glider to travel between the eastern boundary and 200 km, which is our defined western boundary of the Front Current. When presenting the full horizontal wind stress field, the same temporal averaging is used.

2.4 Identification of circulation branches

To distinguish the volume transport of the WSC core, the Front Current branch and the recirculating Atlantic Water, we apply boundaries at 300 and 200 km distance on the target section (indicated between panels a) and c) in Fig. 1). We base the separation of these regions on the structure of the section-averaged meridional velocity fields and their standard deviation shown in Figure 4a, b. This definition is comparable with, e.g., the definitions used by Beszczynska-Möller et al. (2012). While the WSC core and the Front Current can often be clearly distinguished from one another in our data set, i.e., when they merge north of our target section, in some sections these two branches appear as one combined northward flowing current. Attempts to isolate the two current cores in all sections using an automated routine failed, requiring complex methods and subjective choices. Therefore, we consider that the simple fixed boundaries along the transect is a reasonable choice. Applying the same vertical boundaries gives a consistent lateral extent for currents in all sections, making the volume transport estimates between different occupations directly comparable.

2.5 Volume transport estimates

For each section, the volume transport, Q, is estimated as

$$Q = \sum v_g(x,z)\Delta x \Delta z, \tag{1}$$

where $v_g(x,z)$ is the absolute geostrophic velocity directed northward, perpendicular to the section, $\Delta x = 2000\,\mathrm{m}$ and $\Delta z = 1.97\,\mathrm{m}$ (we used 2 dbar vertical bins). The resulting estimates are given in Sverdrup, where $1\,\mathrm{Sv} \equiv 10^6\,\mathrm{m^3\,s^{-1}}$. Different condi-

https://doi.org/10.5194/egusphere-2025-6340
Preprint. Discussion started: 30 December 2025

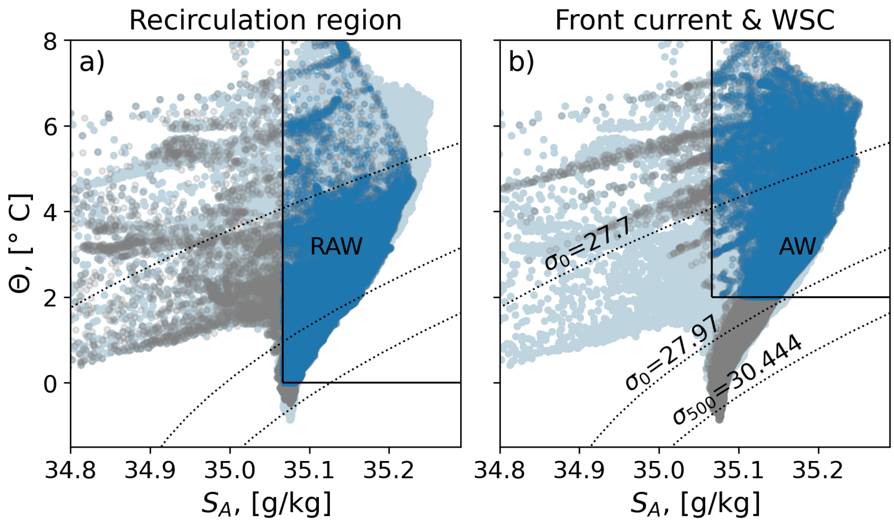

Figure 3. $\Theta - S_A$ diagrams for the a) recirculation region and b) the Front Current and WSC, i.e., west and east of 200 km, respectively (grey dots). Temperature and salinity that corresponds to a) recirculating Atlantic Water (RAW) and b) Atlantic Water (AW) are highlighted in blue. The light blue markers in the background are the same in both panels for reference. Every fifth data point is shown.

tions are applied to the data fields before estimating different parts of the transport across the target section. The transport over the full vertical extent of measurements, independent of water mass classification, is indicated by Q, and calculated separately for the identified branches: $0-200\,\mathrm{km}$ for recirculation, $200-300\,\mathrm{km}$ for the Front Current, and $>300\,\mathrm{km}$ for the WSC.

Θ – S_A diagrams for all missions and separated into the recirculation region and the Front Current/WSC region are shown in Fig. 3 together with water mass definitions. Volume transport of Atlantic Water, Q_{AW}, is calculated within the WSC core and the Front Current, using the data points with northward velocities and with temperatures above 2°C and $S_A > 35.06\,\mathrm{g\,kg^{-1}}$ (indicated in Fig. 3b), consistent with Beszczynska-Möller et al. (2012).

Volume transport of recirculating Atlantic Water (Q_{RAW}) is calculated in the region west of 200 km. Within the recirculation region we estimate the volume transports of both northward and southward flowing warm water as we expect that warm water flowing northward at these longitudes might eventually recirculate farther north in Fram Strait, and ultimately be brought southward instead of entering the Arctic Ocean (e.g., Hattermann et al., 2016; Hofmann et al., 2021; Wekerle et al., 2017). When presenting estimates of Q_{RAW} we indicate the northward and southward components separately. The magnitude of the largest of the two estimates may serve as a potential upper limit of the total Q_{RAW} in the part of Fram Strait covered by the gliders. The same salinity limit as for Atlantic Water is applied, but the temperature threshold is lowered to 0°C following the water mass classification of RAW by Rudels et al. (2005). The water mass classification and the data selected as RAW are highlighted in Fig. 3a. We do not apply the density limits of $\sigma_0 > 27.97$ for RAW and $\sigma_0 > 27.7$ for AW as this disregards much of the near-surface warm water that is saline enough to be Atlantic Water (Fig. 3). Note that southward flowing Atlantic Water east of 200 km, e.g., due to eddies, is not included in our estimate of recirculating Atlantic Water.

https://doi.org/10.5194/egusphere-2025-6340
Preprint. Discussion started: 30 December 2025

The glider does not always cover the full target section. Consequently, the volume transport of the most eastern and western regions cannot always be estimated directly. To directly compare the volume transport of all the sections, however, the transect area should always be the same. We, therefore, approximate the average AW and RAW volume transport as a function of zonal distance using all the sections. These estimates are then used to fill the missing edges of the sections that do not sample the complete target transect. The average added volume transport is 1.6% of the total volume transport for the WSC core estimate (east of $300\,\mathrm{km}$), 2.1% for the Front Current region ($200-300\,\mathrm{km}$), and 16.6% for the recirculation region (west of $200\,\mathrm{km}$). Sections with no data in the relevant regions are omitted from these estimates. Out of the total 22 sections, two sections had less than 75% data coverage in the WSC and the Front Current regions while eight sections had less than 75% data coverage in the recirculation region.

3 Results and discussion

The gliders repeated the target section 22 times during the autumn and winter seasons of 2020, 2021, and 2022. Atlantic Water was present throughout all missions and reached a maximum temperature of $9.2°$C in early autumn 2022. The highest salinity, $35.2\,\mathrm{g\,kg^{-1}}$, was recorded during the subsequent section, while the maximum velocity of $60\,\mathrm{cm\,s^{-1}}$ occurred the previous year, in November 2021. The coldest water masses observed were sufficiently dense to meet the Norwegian Sea Deep Water characteristics as defined by Rudels et al. (2005). These water masses were only detected within the WSC and Front Current regions (Fig. 3).

In the following we first present the average structure in the observed transect, followed by volume transport estimates of AW and RAW. We next discuss the temporal variability, in particular in relation to wind forcing. Wind stress across the target transect is generally directed southwestward, with an average absolute magnitude of $0.08\,\mathrm{N\,m^{-2}}$ (Fig. 2). A pronounced seasonal cycle is evident from 2020 through 2022, with strong southward wind stress reaching nearly $0.3\,\mathrm{N\,m^{-2}}$ in spring. Only the onsets of these high-stress periods are captured at the end of glider missions two and three (Fig. 2a). The strong wind stress observed at the end of mission three in 2022 forms the basis of one of the two case studies further discussed in Section 3.4.

3.1 The average state

The composite average of the absolute geostrophic velocity, temperature and salinity are presented in Fig. 4, together with their standard deviations over the different occupations. The WSC and the Front Current are both clearly represented in the average velocity sections (Fig. 4a). On average, the WSC is centered over the $1100\,\mathrm{m}$ isobath and brings AW northward at a mean velocity of $14.6\,\mathrm{cm\,s^{-1}}$, with a standard deviation of $9.9\,\mathrm{cm\,s^{-1}}$. The Front Current is positioned between approximately 230 and $280\,\mathrm{km}$ in the average section, however, its strength, width, and location vary considerably, as indicated by the large standard deviation between the two current cores (Fig. 4a,b). Consequently, the two branches are sometimes separated and at other times merged.

https://doi.org/10.5194/egusphere-2025-6340
Preprint. Discussion started: 30 December 2025

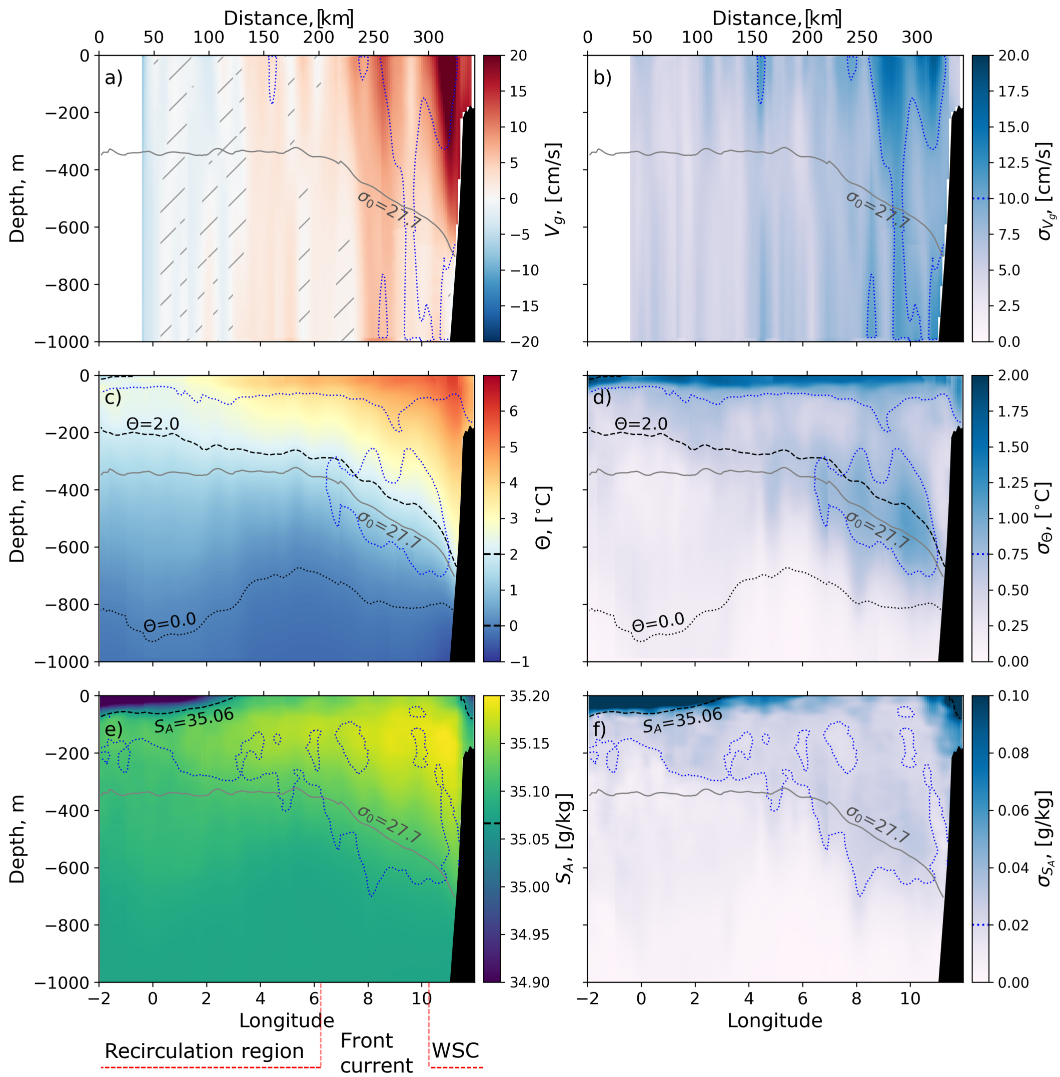

Figure 4. Average (left column) and standard deviation (right column) fields of the a,b) geostrophic velocity, v_g, (positive northward), c,d) temperature, Θ, and e,f) salinity, S_A, based on the 22 glider sections. In a) absolute velocities less than $1\,\mathrm{cm\,s^{-1}}$ are hatched. Average contours of $\sigma_0 = 27.7$, $\Theta = 2.0$ and $0.0°\mathrm{C}$ and $S_A = 35.06$ are indicated. Blue dotted contours indicate standard deviation of a,b) $\sigma_{v_g} = 10\,\mathrm{cm\,s^{-1}}$, c,d) $\sigma_\Theta = 0.75°\mathrm{C}$, and e,f) $\sigma_{S_A} = 0.02$. Below panel e) the regions of Recirculation, Front Current, and the WSC are indicated.

Average properties and volume transports during autumn and winter, computed over the selected branches, are listed in
215 Table 2. In these calculations the averaging is not constrained by water mass criteria. The current is clearly enhanced in winter relative to autumn ($12.2\,\mathrm{cm\,s^{-1}}$ vs. $9.9\,\mathrm{cm\,s^{-1}}$), in agreement with Beszczynska-Möller et al. (2012). The velocity-weighted mean temperature of the WSC branch increases from $3.72\,°\mathrm{C}$ in winter to $4.56\,°\mathrm{C}$ in autumn. Further west, in the Front Current, the temperatures in winter and autumn are not significantly different, and are $1-2\,°\mathrm{C}$ colder than in the WSC region. In the

https://doi.org/10.5194/egusphere-2025-6340
Preprint. Discussion started: 30 December 2025

Table 2. Volume transport (Q), velocity-weighted mean temperature (Θ) and salinity (S_A), and mean velocity (v_g) during the glider missions, computed over the selected circulation branches from the average autumn and winter fields. N denotes the number of sections included in each average with more than 75% data coverage. The total number of sections is 10 for autumn and 11 for winter. Calculations are over the horizontal extent of the branches and the full vertical extent of the measurement, not constrained by water mass criteria.

	$Q\pm$ std, [Sv]		Θ [°C]		S_A		v_g [cm s^{-1}]		N	
	Autumn	Winter	Autumn	Winter	Autumn	Winter	Autumn	Winter	Autumn	Winter
WSC region	2.7±1.8	3.5±1.8	4.56	3.72	35.17	35.15	9.4	12.2	9	10
Front Current region	4.9±3.1	4.8±3.6	2.72	2.74	35.14	35.15	4.8	4.6	10	9
Northward recirculation	0.7±0.9	2.6±2.6	1.24	1.61	35.10	35.11	3.9	5.0	7	7
Southward recirculation	-1.8±1.8	-0.9±1.4	1.27	0.92	35.10	35.10	-4.4	-4.8	7	7

recirculation region, the northward transport increases 3 to 4 times in winter relative to autumn, however, both average values are enveloped by equally large standard deviations, highlighting the large variability.

The average temperature and salinity fields illustrate how the warm AW of the WSC closely follows the continental shelf break, where AW reaches depths of approximately 600 m (Fig. 4c,e). The highest average temperatures, up to $6.14\,°\mathrm{C}$, occur near the shelf break, while waters warmer than $2\,°\mathrm{C}$ extend across the entire transect. The standard deviation of the temperature field highlights variability in the vertical extent of the thermocline. Differences in water mass properties east and west of 200 km are evident in $\Theta - S_A$ space: the warmest and most saline waters are found within the Front Current and the WSC (Fig. 3).

3.2 Volume transport: Atlantic Water and recirculation

Volume transport estimates for AW (in the WSC and Front Current) and RAW in the recirculation region are listed in Table 3 for autumn, winter and over all sections. On average, the northward volume transport of Atlantic Water, Q_{AW}, in the WSC

Table 3. Volume transport (Q) during the average autumn, winter, and total average fields constrained by water mass criteria. Section nr 14 is not included in the total estimate since it lasted from 7$^{\text{th}}$ to 15$^{\text{th}}$ of August, which is neither winter nor autumn.

	$Q\pm$ std, [Sv]		
	Autumn	Winter	Total
WSC region - Q_{AW}	2.5±1.3	2.9±1.5	2.7±1.4
Front Current region - Q_{AW}	2.6±1.7	2.7±2.2	2.6±2.0
Northward recirculation - Q_{RAW}	0.5±0.7	1.9±2.1	0.9±1.7
Southward recirculation - Q_{RAW}	-1.6±1.4	-0.7±1.0	-0.9±1.3

https://doi.org/10.5194/egusphere-2025-6340
Preprint. Discussion started: 30 December 2025

is 2.7 Sv, and in the Front Current 2.6 Sv, identical to within 0.1 standard deviation. While the transport of the two currents are typically comparable, some sections result in significantly larger Q_{AW} in the Front Current, e.g. in Jan 2022 and Aug-Sep 2022 (Fig. 5a).

For comparison, the long-term mean (1997–2010) net volume transport of water warmer than 2°C (same temperature limit as in our analysis) at the Fram Strait mooring array is 3.0 ± 0.2 Sv (Beszczynska-Möller et al., 2012), with 1.3 ± 0.1 Sv carried in the WSC core and showing no seasonal variability. The lack of seasonal variability implies that the near zero Q_{AW} estimates in WSC in our data (e.g., Jan and Sep 2022) are likely because the core is displaced out of the zone selected for this branch and potentially merged with the Front Current, or temporarily suppressed. In both these occurrences, the Front Current has enhanced transport (Fig. 5a). Assuming our limited observations are representative for a longer term average, the large difference between our estimates of total Q_{AW} (5.3 Sv) and the mooring-based transport (3 Sv), further implies that approximately 2 Sv of AW must have been lost to recirculation between $77°15' - 79°$N. This agrees with the recirculation estimate by Marnela et al. (2013).

Transport estimates in temperature–salinity bins, presented in $\Theta - S_A$ space, show largest volume transports in the Atlantic Water class between the 27.7 and 27.97 isopycnals (Fig. 6c). As the barotropic component generally dominates the northward current (Fig. A2), there is also a substantial northward transport of the deeper cold and denser water masses (Fig. 6c and Fig. A3). There is a clear distinction in water mass density classes transported by the WSC and the Front Current (Fig. A3). The WSC transports a relatively broad density range centered around $\sigma_0 = 27.75\,\mathrm{kg\,m^{-3}}$, while the Front Current carries denser waters characterized by two narrow peaks: one centered at approximately $\sigma_0 = 27.9$, and one at $\sigma_0 = 28.05\,\mathrm{kg\,m^{-3}}$. This is a manifestation of the different water mass modifications the slope and front branches of the Norwegian Atlantic Current experience as they move poleward. Huang et al. (2023) showed that in the mean state from 2005 to 2018, air-sea heat flux accounts almost entirely for the net cooling of AW along the Front Current, while oceanic lateral heat transfer appears to dominate the temperature change along the Slope Current. At approximately 77°N, before the two branches merge in Fram Strait, the average density of the Slope Current is about 27.8 whereas the Front Current is $27.9\,\mathrm{kg\,m^{-3}}$ (their Fig. 2e). Similarly, Walczowski (2013) presents the 1996–2007 summer mean transect along $76°30'$N (his transect 'N' and Fig. 5.6), at a location before the different branches converge. Two zones of baroclinicity and resulting baroclinic currents are clearly distinct: above the Knipovich Ridge (the Front Current) and above the Spitsbergen slope (the WSC core), with the front branch approximately 0.1 to $0.15\,\mathrm{kg\,m^{-3}}$ denser. Our observations are thus consistent with these analyses.

West of 200 km, in the region of recirculation, there is relatively strong transport both northward and southward (Fig. 5 and Fig. 6a,b). The average volume transport of RAW is 0.9 Sv northward and −0.9 Sv southward. This could amount to a total recirculation of 0.9 Sv assuming that the northward flowing RAW within the defined recirculation region follows the recirculation branch at about 78°N (Hattermann et al., 2016; Hofmann et al., 2021), veering westward and ultimately flowing south, captured again at the western part of our glider transect. Near our transect's latitude, eddy-resolving model studies locate the equatorward limb of the southern recirculation branch between $0 - 3°$W, near the 3000-m isobath, and of the northern recirculation branch between $3 - 5°$W, near the 2000-m isobath (Wekerle et al., 2017, e.g., their fig. 7). It is therefore likely that the glider sections do not capture the full southward recirculation as the glider often had to turn west of the Prime Meridian

https://doi.org/10.5194/egusphere-2025-6340
Preprint. Discussion started: 30 December 2025

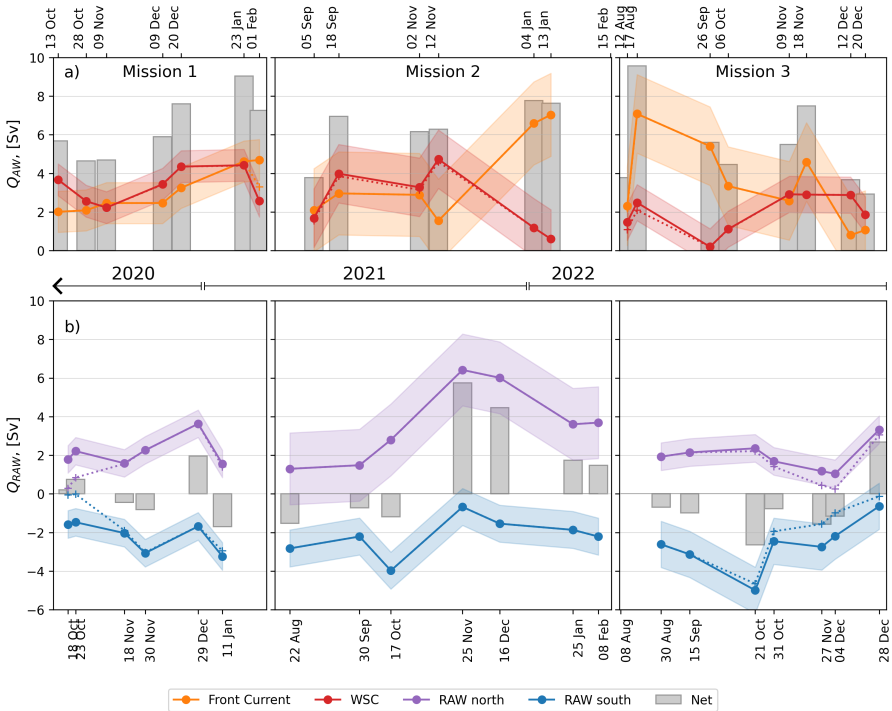

Figure 5. Volume transport, Q, of a) Atlantic Water (AW) and b) Recirculating Atlantic Water (RAW) separated into a) northward Q_{AW} within the WSC (red) and the Front Current (orange) and b) northward (purple) and southward (blue) Q_{RAW}. Grey bars indicate net transport in each panel. Colored shading represents the standard deviation of the transports. Dates correspond to the temporal midpoint of the glider's transit across each domain (east of 200 km for AW and west of 200 km for RAW). Sections not fully sampled by the glider are extrapolated using the average volume transport, except section 14 for Q_{AW} and sections 7 and 15 for Q_{RAW}, which are omitted due to missing data in the eastern and western domains, respectively. Estimates without extrapolation are shown as dotted lines in the respective colors. Note that the x-axes of the two rows align, although the time labels differ, and that there is five to six months gap between missions.

because of sea ice in the region. Since the glider target section was at 77°15′, i.e., upstream of where the Front Current and the WSC tends to merge and south of where the northern recirculation branch is expected to diverge from the slope current (Hattermann et al., 2016; Wekerle et al., 2017), it is also likely that our northward recirculation transport is an underestimate.

While the northward and southward transports nearly balance for most sections (Fig. 5b), the properties of the waters they carry differ markedly (Fig. 6a,b). This indicates that these transport components are not isolated eddies or other reversible flow across the glider transect. The northward transport is warmer and more saline than the southward transport (shift from orange to blue contours in Fig. 6a,b). This change in water mass properties suggests a coherent recirculation pattern, where relatively warm northward-flowing waters are modified during their southward return, cooling and mixing with colder, fresher waters along the path.

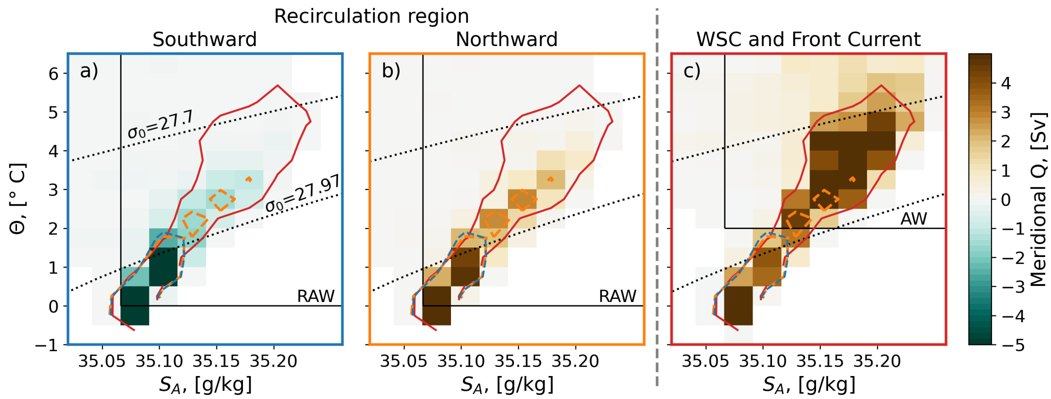

Figure 6. Volume transport in $\Theta - S_A$ space for a) southward and b) northward velocities in the Recirculation region west of 200 km, and c) the full velocity field east of 200 km covering WSC and the Front Current. Vertical and horizontal black lines indicate salinity and temperature limits for RAW a,b) and AW c). Colored contours correspond to the borders of each panel and indicate volume transport of 2 Sv southward (blue) and northward (orange) in the recirculation region, and in the WSC and Front Current region (red). These contours are the same in all three panels.

3.3 Temporal variability of volume transport

Since the gliders traversed the target section repeatedly over three years, we discuss the presence of seasonal and interannual patterns. Complementing the overview of volume transport estimates per branch and section presented in Fig 5, Fig. 7 illustrates the distribution of volume transport across the transect for each section, highlighting variability in the position of the circulation cores. During 2020 and 2022 there appears to be systematically higher transport of AW within the WSC during winter than autumn (Fig 5), in agreement with Beszczynska-Möller et al. (2012). However, this was not the case during mission number two, when the AW transport in the WSC was relatively high both during crossings in September and November, and low in January.

During both mission number two and the beginning of mission number three, there is a tendency that the Front Current transport is weaker when the WSC is stronger, and vice versa. These periods of reduced WSC might reflect temporary suppression of the WSC or meandering of the current core. A reduced amount of water warm and saline enough to be considered AW could also explain the low AW volume transport, however, the area of AW present in the WSC region remains relatively stable throughout the glider sections (not shown). Conversely, in the Front region, the cross-sectional area of AW does co-vary with the AW volume transport. During sections 12 and 13 at the end of mission number two, when Q_{AW} is anomalously weak in the WSC region (Fig. 7a), the $\sigma_0 = 27.97$ isopycnal is deep (roughly 700 m) and flat (not shown), supporting a large volume of AW in both the Front Current and WSC regions, but with low WSC velocities. This suggests that the current speed is the limiting factor of AW transport in the WSC region, while volume of AW is the limiting factor in the Front region. While the divide between the Front Current and WSC regions at 300 km appears to be a robust choice (Fig. 4 and Fig. 7), these two

https://doi.org/10.5194/egusphere-2025-6340
Preprint. Discussion started: 30 December 2025

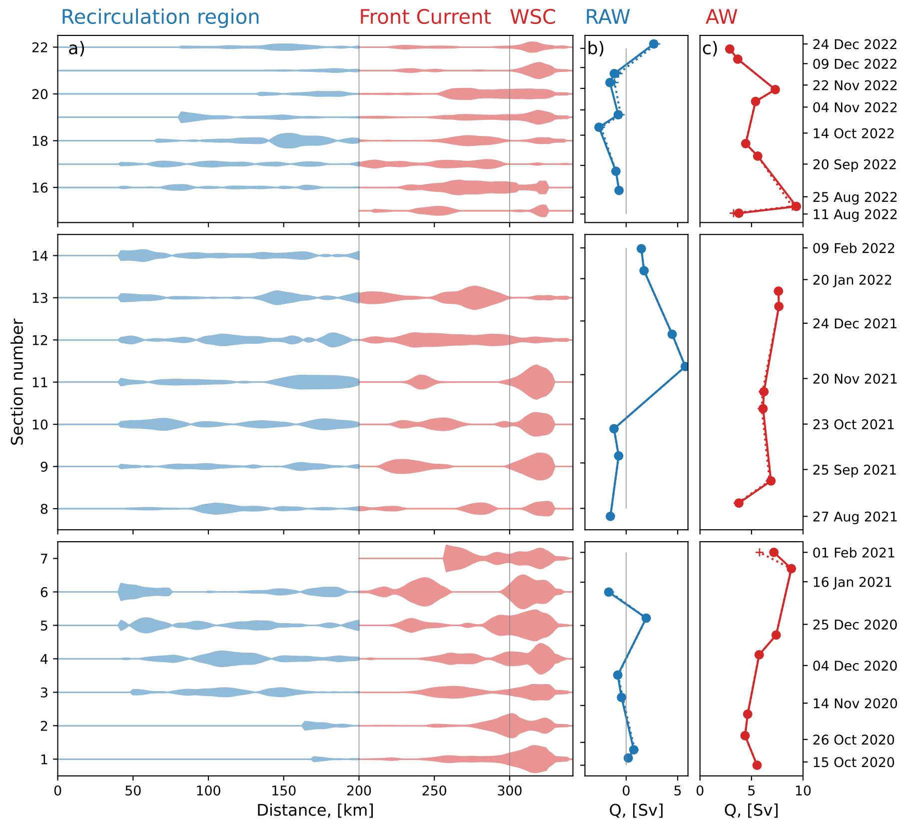

Figure 7. The volume transport of recirculating Atlantic Water (Q_{RAW}, blue) and northward-flowing Atlantic Water (Q_{AW}, red). a) The zonal variability of Q_{RAW} west of 200 km (blue) and Q_{AW} east of 200 km (red) for each section. The volume transport is mirrored over the horizontal axis to emphasize the zonal variability. The actual magnitude of the volume transport is not shown in this panel. The zonally summed b) Q_{RAW} and c) Q_{AW} with (solid) and without (dotted) extrapolation of unsampled regions. The dates along the vertical axis of panel c) are the temporal midpoints of each section.

current cores do merge (e.g., sections 2, 5, 12) and shift (e.g., sections 13 and 17) across this divide during some sections (Fig. 7), thus contributing to the apparent fluctuation between strong Q_{AW} in the Front Current and the WSC during some instances.

In the recirculation region there is a tendency for co-variability between the northward and southward component (Fig. 5b). This indicates that the region is either dominated by northward current or southward current, rather than that the domain is split in two with northward current furthest east and southward current in the west. For most sections, the net volume transport of RAW is directed southward. The main exception is in November and December 2021, when there is a strong ($> 4\,\mathrm{Sv}$) northward transport of RAW also in the recirculation region.

https://doi.org/10.5194/egusphere-2025-6340
Preprint. Discussion started: 30 December 2025

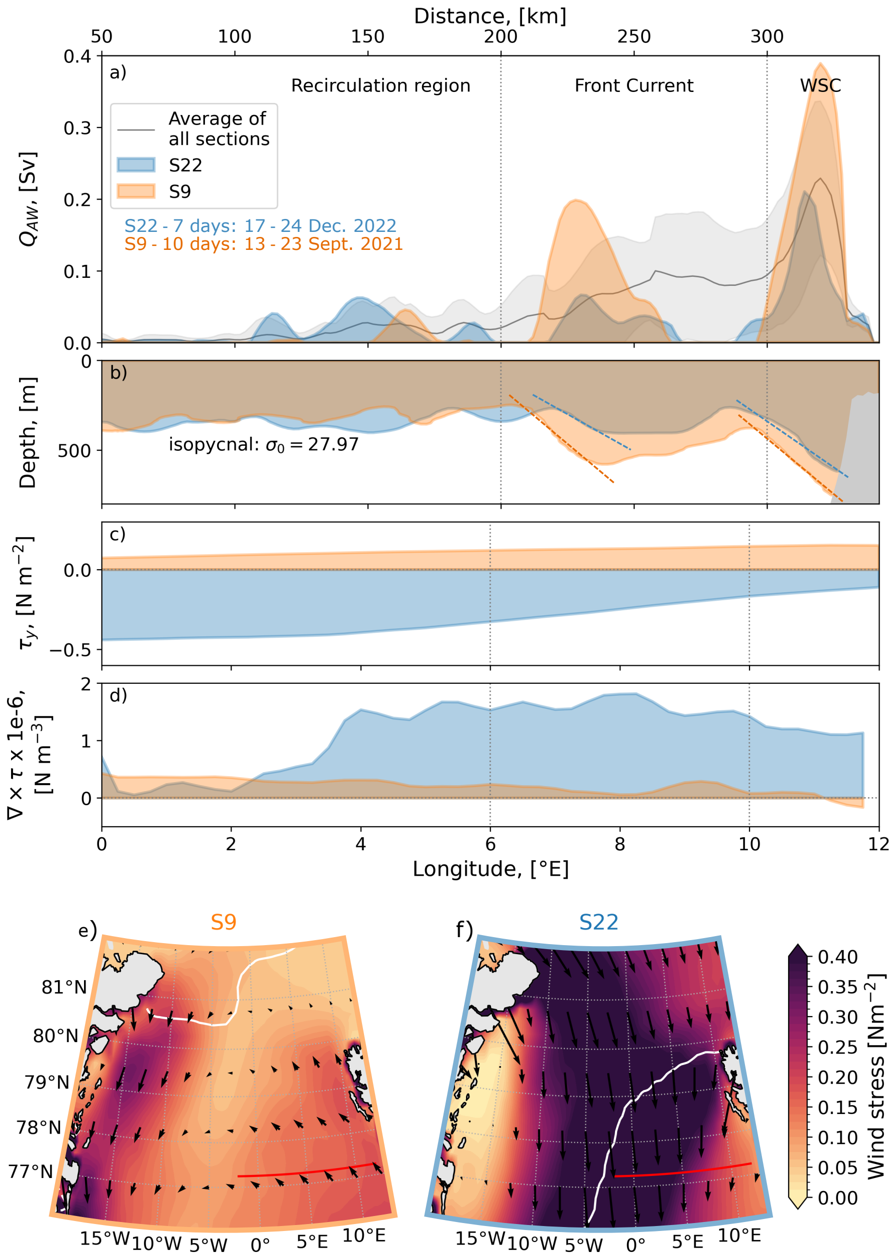

Figure 8. a) AW volume transport and b) the $\sigma_0 = 27.97$ isopycnal depth of glider sections 9 (S9, orange) and 22 (S22, blue). The gray line and shading in panel a) are the average and standard deviation over all sections. The colored dashed lines in panel b) indicate the slopes of the fronts supporting the WSC and the Front Current. Average c) meridional wind stress and d) wind stress curl over $77.25°\mathrm{N} \pm 0.75°$ and the full wind stress field for e) section 9 and f) section 22 during the time it took the glider to cross the distance spanning from 200 km on the target transect to the eastern boundary for sections 9 and 22. White contour is the sea ice edge and the red line is the target transect.

https://doi.org/10.5194/egusphere-2025-6340
Preprint. Discussion started: 30 December 2025

3.4 Case study: Atmospheric forcing of Q_{AW} variability

To investigate potential drivers of the variability in Q_{AW}, we identify two periods of distinctly different wind stress forcing over the glider section (Fig. 8). During September 2021, the wind stress was anomalously strong northward and aligned with the shelf break, while during December 2022, the wind stress was anomalously strong southward (Fig. 8c-f).

During the northward wind stress anomaly, the maximum AW volume transport per 2-km bin within the WSC is nearly twice as strong as the average (Fig. 8a, orange). There is also a clear core within the Front Current region, and these two current cores are distinctly separated. During the period when southward wind stress dominates, the WSC is weaker and the outer core is nearly disintegrated (Fig. 8a, blue). In agreement with the different magnitudes of AW volume transport during the two sections, the 27.97 isopycnal is steeper in both the Front Current and the WSC regions in September 2021 when the volume transport is strongest (Fig. 8b). This suggests that the observed difference in AW volume transport is at least partly baroclinically driven.

The reduced WSC strength during December 2022 might be a direct result of the anomalous wind stress through positive meridional gradients (Fig. 2 and 8c,d) and resulting Ekman transport away from the coast which i) lifts and flattens the isopycnals reducing the baroclinic current component, and ii) reduces the sea surface anomaly towards the coast which reduces the barotropic current component. Conversely, the northward wind stress during September 2021 likely heightens the sea surface along the coast and steepens the isopycnals, driving both an enhanced northward barotropic and baroclinic current component.

The reduced AW volume transport in the Front Current region during southward stress might be related to open-ocean divergence in the Ekman layer. As the Front Current is $\sim$100 km away from the coast, direct barotropic adjustment is likely not the main explanation for the decreased current. However, just as over the WSC region, the zonal gradient in the meridional wind stress is strongly positive during December 2022 (Fig. 8c,d). This divergence can lift the isopycnals that support the Front Current, which relaxes their slope, and consequently slows down the current. While the average wind stress over the WSC is roughly $-0.15\,\mathrm{N\,m^{-2}}$ during December 2022, the maximum southward wind stress further east is $0.4\,\mathrm{N\,m^{-2}}$, thus setting up a strong gradient and a wind stress curl of almost $2\times10^{-6}\,\mathrm{N\,m^{-3}}$. Comparatively, the wind stress curl during September 2021, when the WSC and Front Current were both strong, was nearly zero, thus yielding minimal impact on the deep isopycnals.

Frank et al. (2025) investigated warm AW intrusions onto the West Spitsbergen Shelf as identified from high-resolution regional model output across zonal cross-shelf sections starting from $77°20'$N, close to our target section. The amplitudes of WSC velocity peaks appear to be reduced during prolonged periods of strong offshore Ekman transport, and the current tends to be positioned further offshore over deeper bathymetry— similar to our case section 22. They emphasize that events of on-shelf AW intrusion were influenced by multiple cross-shelf exchange mechanisms that may act simultaneously (e.g., increase in core speed, displacement of core on the slope, near-surface onshore Ekman transport of warm water, upwelling of deeper waters in response to offshore Ekman transport etc.). Similarly, we could expect multiple processes leading to variability in the relative position, strength and interactions of the Front Current and the WSC.

https://doi.org/10.5194/egusphere-2025-6340
Preprint. Discussion started: 30 December 2025

4 Conclusions

We present estimates of northward transport of warm Atlantic Water across a zonal transect at $77°15'$N based on repeated ocean glider sections. In total, 22 sections were collected during three missions covering autumn and winter in 2020, 2021 and 2022. The fine spatial resolution of the glider transects provides well-resolved circulation cores, lending confidence to the estimated volume transports. Although glider data require more extensive post-processing compared to mooring or ship-based observations, their high spatial resolution offers an advantage over traditional mooring arrays, and repeated seasonal coverage provides an improvement over single ship-based sections.

On average, both the WSC and the Front Current transport approximately $2.5\,\mathrm{Sv}$ of Atlantic Water (AW, $\Theta > 2°\mathrm{C}$, $S_A > 35.06\,\mathrm{g\,kg^{-1}}$) northward during autumn and winter, resulting in a combined transport of about $5\,\mathrm{Sv}$ toward the Arctic. There is an indication of higher AW transport in the WSC during winter compared to autumn, but this difference is not significant within one standard deviation. Additional missions would be required to confirm this apparent seasonality. The elevated winter transport in the WSC coincides with stronger current speeds. Within the Front Current, high AW volume transport also co-varies with the cross-sectional area of warm AW, whereas this is not the case in the WSC region. This suggests that AW availability is a limiting factor for the Front Current but not in the WSC during autumn and winter.

Two cases of anomalous surface wind stress are examined. During the event with strong northward stress over the WSC and Front Current regions, northward transport of warm Atlantic Water is enhanced: both the maximum Q_{AW} in the WSC and the Front Current are approximately twice their respective average values. This is consistent with the expected Ekman dynamics, where northward wind stress west of Svalbard elevates sea surface height along the coast and strengthens northward barotropic currents. Conversely, during the event with a strong southward wind stress, the WSC weakens and the Front Current nearly disintegrates. During this period, the wind stress curl is positive, suggesting that both lifting of isopycnals and reduced sea surface height anomalies likely contribute to the weakened currents.

Our target section partly captured the southern, weaker recirculation branch in Fram Strait. The net volume transport of recirculating Atlantic Water (RAW, $\Theta > 0°\mathrm{C}$, $S_A > 35.06\,\mathrm{g\,kg^{-1}}$) west of the Front Current is close to $0\,\mathrm{Sv}$, i.e., the northward and southward average transports approximately balance. However, the properties of the waters they carry indicate a coherent recirculation pattern, where relatively warm northward-flowing waters are modified during their southward return, cooling and mixing with colder, fresher waters along the path. Under this assumption, we estimate the strength of the recirculation at the observed section to be approximately $1\,\mathrm{Sv}$.

This study demonstrates the capability of ocean gliders as observing platforms – even in regions of strong boundary currents. The pronounced variability in the strength, structure, and position of both the WSC and the Front Current could not be captured by a reasonably spaced mooring array. This variability appears to reflect atmospheric conditions; however, because the strongest wind stress typically occurs in spring and summer, i.e., between the glider deployments presented here, we cannot assess the most anomalous Q_{AW} conditions. A mission program extending through summer as well as winter would provide critical insight into current core dynamics and Q_{AW} under such atmospheric forcing, particularly for the Front Current, which is not constrained by the continental shelf break.

https://doi.org/10.5194/egusphere-2025-6340
Preprint. Discussion started: 30 December 2025

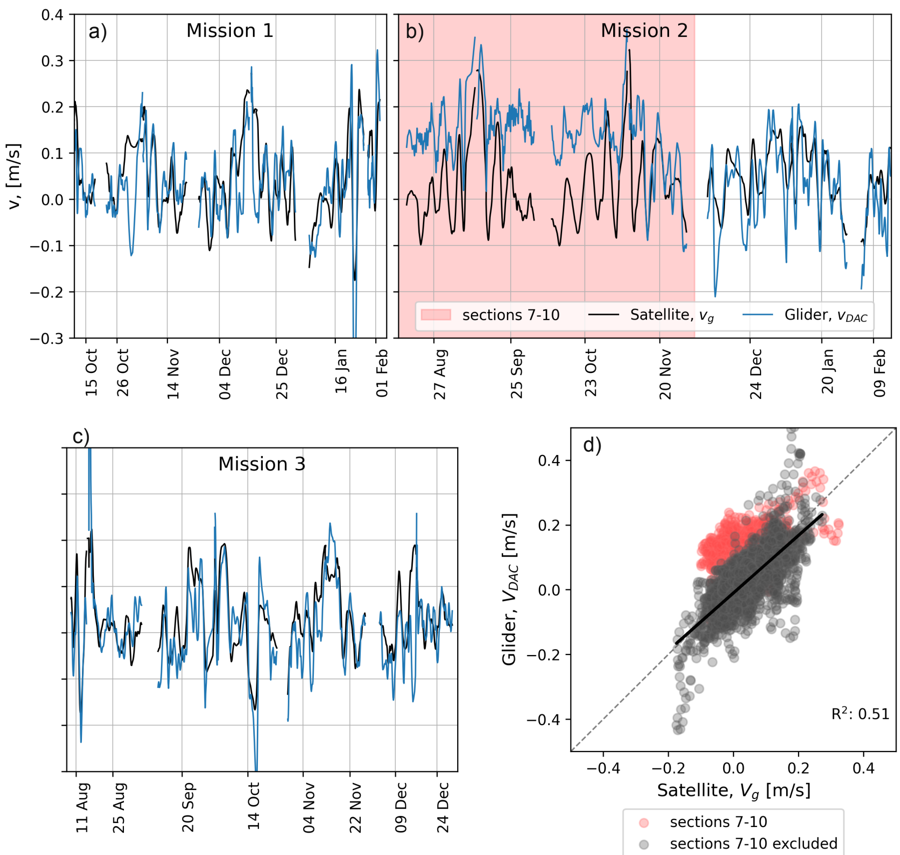

Figure A1. a-c) Time series and d) scatter plot of the northward surface geostrophic current (Satellite, v_g) versus the northward component of the depth-averaged current (DAC) between dives estimated by the gliders (Glider, v_{DAC}). In b,d) the pale red region and markers indicate sections seven through ten where v_{DAC} was suspiciously strong over large parts of the target section. The value of R^2 in d) is estimated based on data points excluding sections seven through ten, and the dashed grey line indicates the perfect agreement for reference.

Appendix A: Supporting figures

The depth-averaged current (DAC) estimated by the gliders agree with the currents we expect from this region for most of the missions, except for roughly half the sections during mission 2. These sections have strong northward DAC estimates ($> 10\,\mathrm{cm\,s^{-1}}$) across most of the section (Fig. A1b). We compared the DAC estimates to surface geostrophic currents from gridded altimeter product (Global Ocean Gridded L4 Sea Surface Heights And Derived Variables Reprocessed 1993 Ongoing, 2024) and concluded that these two estimates compare well except in the period with anomalously high velocities during mission 2 (Fig. A1). While we could not identify the cause, we suspect DAC estimates are erroneous. We therefore use the altimetry based surface geostrophic currents instead of the depth-averaged currents from the glider in our estimates of absolute geostrophic currents for all sections for consistency.

https://doi.org/10.5194/egusphere-2025-6340
Preprint. Discussion started: 30 December 2025

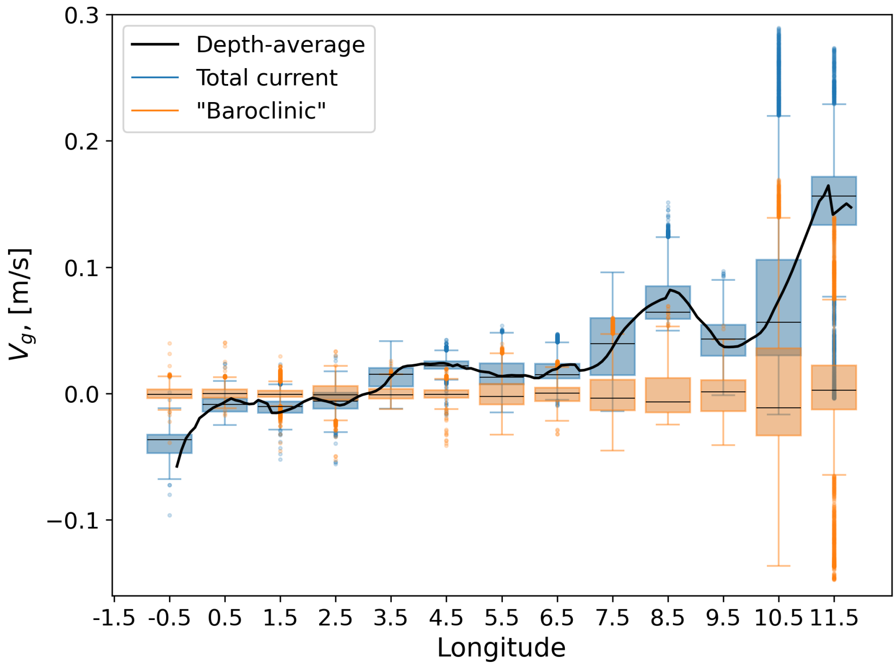

Figure A2. Average current across the target section based on all 22 glider sections. The depth-averaged current (black) and box plots of the depth-varying total current (blue) and the approximated baroclinic current component (total current minus the depth average, orange) in 1° longitude bins. The median of each bin is indicated by horizontal black lines, the box indicates the quartiles, the whiskers indicate the remaining distribution, and the dots are outliers as defined by Seaborn's boxplot function (Waskom, 2021).

The barotropic and baroclinic current components can be approximated as the depth-averaged current and as the depth-averaged current subtracted from the full current field, respectively (Fig. A2). The velocities are consistently higher in the approximated barotropic component than in the baroclinic component when considering the velocity field averaged over all 22 glider sections (Fig. A2). The same is true for nearly all periods both spatially and temporally when considering each section individually (not shown).

The different regions (WSC, Front Current and Recirculation) carry different water masses across the transect. Both the WSC and the Front current have a net northward transport within all density classes, including the densest registered water masses (Fig. A3). The WSC brings the lightest AW northward: its distribution peaks at roughly $\sigma_0 = 27.75$, while the Front current brings denser AW northward, peaking at almost $\sigma_0 = 27.90$ (Fig. A3). Both within the Front Current and the Recirculation region there is a clear spike in the densest water mass, with approximately $\sigma_0 = 28.05$ (Fig. A3) and $\Theta = 0°C$ (Fig. 6). A small negative peak indicates net southward volume transport in the recirculation region at approximately $\sigma_0 = 28.0$.

https://doi.org/10.5194/egusphere-2025-6340
Preprint. Discussion started: 30 December 2025

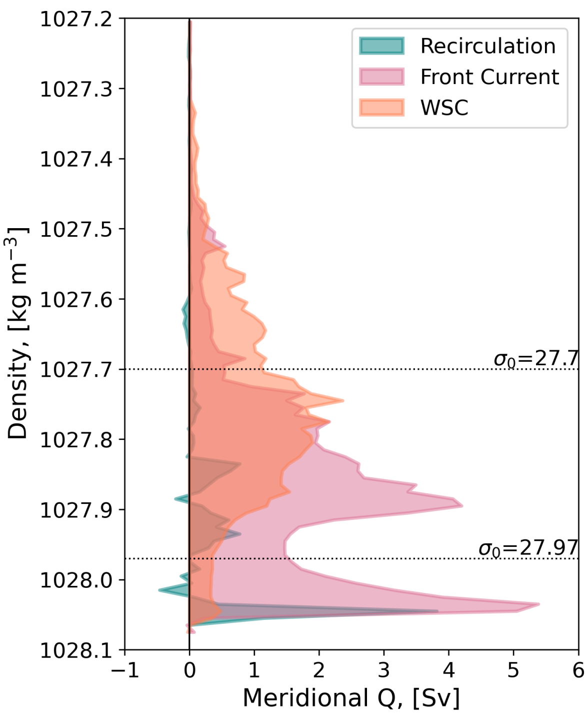

Figure A3. Meridional volume transport as a function of potential density classes for the Recirculation region (teal), the Front Current region (pink), and the WSC region (orange). Selected σ_0 values are indicated.

https://doi.org/10.5194/egusphere-2025-6340
Preprint. Discussion started: 30 December 2025

Data availability. Glider data are available at the Norwegian Marine Data Centre from Fer et al. (2025), https://doi.org/10.21335/NMDC-1222822416. The surface geostrophic-current data set is from the product SEALEVEL_GLO_PHY_L4_MY_008_047, publicly available from the E.U. Copernicus Marine Service Information at https://doi.org/10.48670/moi-00148 (Global Ocean Gridded L4 Sea Surface Heights And Derived Variables Reprocessed 1993 Ongoing, 2024). Atmospheric and sea ice data are obtained from Copernicus Climate Change Service (Hersbach et al., 2023). Bathymetry data is from IBCAO Ver. 4.0 (Jakobsson et al., 2020).

Code and data availability. The data are processed using the Seaglider Basestation3 software (version 3.0.4, https://github.com/iop-apl-uw/basestation3/), which is developed at the University of Washington and maintained by the Integrative Observational Platforms (IOP) group at APL-UW. The GliderTools package for Python is available from Gregor et al. (2019).

Author contributions. IF conceived and planned the experiment, led the glider mission and finalized the processing of glider data. VD developed and performed the analysis with input from IF. VD wrote the paper with feedback from IF. Both authors discussed the results and finalized the paper.

Competing interests. Ilker Fer is a member of the editorial board of Ocean Science.

Acknowledgements. This work was supported by the Research Council of Norway, project number 269927, Svalbard Integrated Arctic Earth Observing System - Infrastructure development of the Norwegian node (SIOS InfraNOR) and project number 328941 (KeyPOCP). The glider was operated by the Norwegian facility for ocean gliders (NorGliders) at the Geophysical Institute, University of Bergen. We thank the NorGliders team, and the scientists and crew of deployment and recovery cruises. Ailin Brakstad performed the delayed-mode reprocessing of the glider data using basestation v3. Gillian M. Damerell and Helene Olsen contributed with processing, quality control and post-mission calibration of a previous version of the glider data.

https://doi.org/10.5194/egusphere-2025-6340
Preprint. Discussion started: 30 December 2025

References

Aagaard, K., Foldvik, A., and Hillman, S. R.: The West Spitsbergen Current- Disposition and water mass transformation, J. Geophys. Res., 92, 3778–3784, 1987.

Beszczynska-Möller, A., Fahrbach, E., Schauer, U., and Hansen, E.: Variability in Atlantic water temperature and transport at the entrance to the Arctic Ocean, 1997-2010, ICES Journal of Marine Science, 69, 852–863, https://doi.org/10.1093/icesjms/fss056, 2012.

Dale, D., Christl, M., Vockenhuber, C., Macrander, A., Ólafsdóttir, S., Middag, R., and Casacuberta, N.: Tracing Ocean Circulation and Mixing From the Arctic to the Subpolar North Atlantic Using the 129I–236U Dual Tracer, J. Geophys. Res., 129, e2024JC021 211, https://doi.org/10.1029/2024JC021211, 2024.

Eriksen, C. C.: Seaglider: a long-range autonomous underwater vehicle for oceanographic research, IEEE J. of Oceanic Eng., 26, 2001.

Fer, I., Peterson, A. K., and Nilsen, F.: Atlantic Water Boundary Current Along the Southern Yermak Plateau, Arctic Ocean, J. Geophys. Res., 128, e2023JC019 645, https://doi.org/10.1029/2023JC019645, 2023.

Fer, I., Brakstad, A., Damerell, G. M., and Elliott, F.: Physical oceanography data from Seaglider missions west of Svalbard, October 2020 - February 2023 [dataset]. Norwegian Marine Data Centre, https://doi.org/10.21335/NMDC-1222822416, 2025.

Frank, L., Albretsen, J., Skogseth, R., Nilsen, F., and Jonassen, M. O.: Mechanisms of warm-water intrusions onto the West Spitsbergen Shelf during winter, Ocean Sci., 21, 2419–2442, https://doi.org/10.5194/os-21-2419-2025, 2025.

Global Ocean Gridded L4 Sea Surface Heights And Derived Variables Reprocessed 1993 Ongoing: E.U. Copernicus Marine Service Information (CMEMS). Marine Data Store (MDS) [data set], https://doi.org/10.48670/moi-00148, Accessed on 24 May 2024, 2024.

Gregor, L., Ryan-Keogh, T. J., Nicholson, S.-A., du Plessis, M., Giddy, I., and Swart, S.: GliderTools: A Python Toolbox for Processing Underwater Glider Data, Frontiers in Marine Science, 6(December), 1–13, https://doi.org/10.3389/fmars.2019.00738, 2019.

Hattermann, T., Isachsen, P. E., von Appen, W.-J., Albretsen, J., and Sundfjord, A.: Eddy-driven recirculation of Atlantic Water in Fram Strait, Geophys. Res. Lett., 43, 3406–3414, https://doi.org/10.1002/2016GL068323, 2016.

Hersbach, H., Bell, B., Berrisford, P., Biavati, G., Horányi, A., Muñoz Sabater, J., Nicolas, J., Peubey, C., Radu, R., Rozum, I., Schepers, D., Simmons, A., Soci, C., Dee, D., and Thépaut, J.-N.: ERA5 hourly data on single levels from 1940 to present. Copernicus Climate Change Service (C3S) Climate Data Store (CDS), https://doi.org/10.24381/cds.adbb2d47, Accessed on 30-Jun-2025, 2023.

Hofmann, Z., von Appen, W.-J., and Wekerle, C.: Seasonal and Mesoscale Variability of the Two Atlantic Water Recirculation Pathways in Fram Strait, J. Geophys. Res., 126, e2020JC017 057, https://doi.org/10.1029/2020JC017057, 2021.

Huang, J., Pickart, R. S., Chen, Z., and Huang, R. X.: Role of air-sea heat flux on the transformation of Atlantic Water encircling the Nordic Seas, Nat. Comms., 14, 141, https://doi.org/10.1038/s41467-023-35889-3, 2023.

Ingvaldsen, R. B., Assmann, K. M., Primicerio, R., Fossheim, M., Polyakov, I. V., and Dolgov, A. V.: Physical manifestations and ecological implications of Arctic Atlantification, Nat. Rev. Earth Environ., 2, 874–889, https://doi.org/10.1038/s43017-021-00228-x, 2021.

Jakobsson, M., Mayer, L. A., Bringensparr, C., Castro, C. F., Mohammad, R., Johnson, P., Ketter, T., Accettella, D., Amblas, D., An, L., Arndt, J. E., Canals, M., and Casamor, J. L.: The International Bathymetric Chart of the Arctic Ocean Version 4.0, Scientific Data, 7, https://doi.org/10.1038/s41597-020-0520-9, 2020.

Manley, T. O.: Branching of Atlantic Water within the Greenland- Spitsbergen passage: An estimate of recirculation, J. Geophys. Res., 100, 20,627–20,634, 1995.

Marnela, M., Rudels, B., Houssais, M. N., Beszczynska-Möller, A., and Eriksson, P. B.: Recirculation in the Fram Strait and transports of water in and north of the Fram Strait derived from CTD data, Ocean Sci., 9, 499–519, https://doi.org/10.5194/os-9-499-2013, 2013.

McDougall, J. T. and Barker, P. M.: Getting started with TEOS-10 and the Gibbs Seawater (GSW) Oceanographic Toolbox, 28pp., SCOR/IAPSO WG127, ISBN 978-0-646-55621-5, Tech. rep., 2011.

McPherson, R. A., Wekerle, C., and Kanzow, T.: Shifts of the Recirculation Pathways in Central Fram Strait Drive Atlantic Intermediate Water Variability on Northeast Greenland Shelf, J. Geophys. Res., 128, e2023JC019 915, https://doi.org/10.1029/2023JC019915, 2023.

Mork, K. A. and Skagseth, Ø.: A quantitative description of the Norwegian Atlantic Current by combining altimetry and hydrography, Ocean Sci., 6, 901–911, https://doi.org/10.5194/os-6-901-2010, 2010.

Orvik, K. A. and Niiler, P.: Major pathways of Atlantic water in the northern North Atlantic and Nordic Seas toward Arctic, Geophys. Res. Lett., 29, 1896, https://doi.org/10.1029/2002GL015002, 2002.

Polyakov, I. V., Pnyushkov, A. V., Charette, M., Cho, K.-H., Jung, J., Kipp, L., Muilwijk, M., Whitmore, L., Yang, E. J., and Yoo, J.: Atlantification advances into the Amerasian Basin of the Arctic Ocean, Science Advances, 11, eadq7580, https://doi.org/10.1126/sciadv.adq7580, 2025.

Quadfasel, D., Gascard, J. C., and Koltermann, K. P.: Large-scale oceanography in Fram Strait during the 1984 Marginal Ice-Zone Experiment, J. Geophys. Res., 92, 6719–6728, 1987.

Rudels, B.: Arctic Ocean circulation, processes and water masses: A description of observations and ideas with focus on the period prior to the International Polar Year 2007-2009, Prog. Oceanogr., 132, 22–67, https://doi.org/10.1016/j.pocean.2013.11.006, 2015.

Rudels, B., Björk, J., Nilsson, J., Winsor, P., and Lake, I. andNohr, C.: The interaction between waters from the Arctic Ocean and the Nordic Seas north of Fram Strait and along the East Greenland Current: results from the Arctic Ocean-02 Oden expedition, J. Mar. Syst., 55, 1–30, https://doi.org/10.1016/j.jmarsys.2004.06.008, 2005.

Rudnick, D. L.: Ocean research enabled by underwater gliders, Annual Review of Marine Science, 8, 519–541, https://doi.org/10.1146/annurev-marine-122414-033913, 2016.

Schauer, U., Fahrbach, E., Østerhus, S., and Rohardt, G.: Arctic warming through the Fram Strait: Oceanic heat transport from 3 years of measurements, J. Geophys. Res., 109, 206026, https://doi.org/10.1029/2003JC001823, 2004.

Testor, P., de Young, B., Rudnick, D. L., Glenn, S., Hayes, D., Lee, C. M., Pattiaratchi, C., Hill, K., Heslop, E., Turpin, V., Alenius, P., Barrera, C., Barth, J. A., Beaird, N., Bécu, G., Bosse, A., Bourrin, F., Brearley, J. A., Chao, Y., Chen, S., Chiggiato, J., Coppola, L., Crout, R., Cummings, J., Curry, B., Curry, R., Davis, R., Desai, K., DiMarco, S., Edwards, C., Fielding, S., Fer, I., Frajka-Williams, E., Gildor, H., Goni, G., Gutierrez, D., Haugan, P., Hebert, D., Heiderich, J., Henson, S., Heywood, K., Hogan, P., Houpert, L., Huh, S., E. Inall, M., Ishii, M., Ito, S.-i., Itoh, S., Jan, S., Kaiser, J., Karstensen, J., Kirkpatrick, B., Klymak, J., Kohut, J., Krahmann, G., Krug, M., McClatchie, S., Marin, F., Mauri, E., Mehra, A., P. Meredith, M., Meunier, T., Miles, T., Morell, J. M., Mortier, L., Nicholson, S., O'Callaghan, J., O'Conchubhair, D., Oke, P., Pallàs-Sanz, E., Palmer, M., Park, J., Perivoliotis, L., Poulain, P.-M., Perry, R., Queste, B., Rainville, L., Rehm, E., Roughan, M., Rome, N., Ross, T., Ruiz, S., Saba, G., Schaeffer, A., Schönau, M., Schroeder, K., Shimizu, Y., Sloyan, B. M., Smeed, D., Snowden, D., Song, Y., Swart, S., Tenreiro, M., Thompson, A., Tintore, J., Todd, R. E., Toro, C., Venables, H., Wagawa, T., Waterman, S., et al.: OceanGliders: A Component of the Integrated GOOS, Frontiers in Marine Science, 6, https://doi.org/10.3389/fmars.2019.00422, 2019.

von Appen, W.-J., Schauer, U., Hattermann, T., and Beszczynska-Möller, A.: Seasonal Cycle of Mesoscale Instability of the West Spitsbergen Current, J. Phys. Oceanogr., 46, 1231–1254, https://doi.org/10.1175/jpo-d-15-0184.1, 2016.

Walczowski, W.: Atlantic Water in the Nordic Seas: Properties, Variability, Climatic Importance, Springer Cham, https://doi.org/10.1007/978-3-319-01279-7, 2013.

https://doi.org/10.5194/egusphere-2025-6340
Preprint. Discussion started: 30 December 2025

Walczowski, W., Piechura, J., Osinski, R., and Wieczorek, P.: The West Spitsbergen Current volume and heat transport from synoptic observations in summer, Deep-Sea Res. I, 52, 1374–1391, 2005.

Waskom, M. L.: seaborn: statistical data visualization, Journal of Open Source Software, 6, 3021, https://doi.org/10.21105/joss.03021, 2021.

Wekerle, C., Wang, Q., von Appen, W.-J., Danilov, S., Schourup-Kristensen, V., and Jung, T.: Eddy-Resolving Simulation of the Atlantic Water Circulation in the Fram Strait With Focus on the Seasonal Cycle, J. Geophys. Res., 122, 8385–8405, https://doi.org/10.1002/2017JC012974, 2017.